

Modeling thermionic electron emission from heterogeneous surfaces

Dongzheng Chen,¹ Ryan Jacobs,¹ Dane Morgan¹, and John Booske^{2,a)}

¹Department of Materials Science and Engineering,

University of Wisconsin-Madison, 1509 University Ave, Madison, WI 53706, USA

²Department of Electrical and Computer Engineering, University of Wisconsin-Madison, 1415 Engineering Dr, Madison, WI 53706, USA

a) jhbooske@wisc.edu

Abstract

We present results of a predictive model of the non-uniform thermionic electron emission from spatially heterogeneous material surfaces in a parallel diode. This model includes the effects of 3-D space charge, patch fields, and Schottky barrier lowering. The model predicts the temperature-limited (TL) emission, the full-space-charge-limited (FSCL) emission, and the smooth, rounded transition between TL and FSCL emission regions, which is the so-called “roll-off” or “knee” feature of the emission current density-temperature $J - T$ (Miram) or the emission current density-voltage $J - V$ curves. The results demonstrate that a thermionic emission cathode with a spatial distribution of discrete-valued work functions will have a smooth transition between TL and FSCL regions for both Miram curves and $J - V$ curves. This physics-based model of thermionic emission has demonstrated characteristics in agreement with experimental observations in emission tests, without any empirical equations or *a priori* assumptions of continuous work function distribution. The emission model established here has direct implications for modeling of electron emission from realistic, heterogeneous surfaces, which is a key research area for improved understanding of the interplay of emission physics, cathode materials engineering, and design of devices employing electron emission cathodes.

Text

Thermionic cathodes provide the electron source in numerous vacuum electronic devices (VEDs) applied to civilian, industrial, and scientific applications, such as communication devices, electron microscopes, electron beam lithography, ion thrusters, thermionic energy converters, and free electron lasers.^{1,2} A cathode surface with a single work function value, referred to as a

“uniform cathode” in this article, is the simplest physical model for a thermionic cathode. The physics of thermionic emission from a uniform cathode in a parallel diode has been thoroughly studied. The Richardson-Dushman equation^{3,4} with Schottky barrier lowering⁵ describes the temperature-limited (TL) emission current density of a uniform cathode. The Child-Langmuir law^{6,7} and Langmuir and Fry’s studies^{7,8} provide a model of the full-space-charge-limited (FSCL) emission. Scott’s and Eng’s works^{9,10} unified both the effects of Schottky barrier lowering and space charge and are able to predict the TL-FSCL transition region for a uniform cathode. However, the TL-FSCL transition region predicted from an emission model of a uniform cathode is characterized by a sharp transition. This predicted sharp transition differs markedly from experimental results of actual thermionic cathode emission measurements,¹⁰ which are characterized by a smoother, more gradual TL-FSCL transition in the Miram and the $I - V$ curves. To date, the only models predicting a smooth TL-FSCL transition are not fully physics-based, and instead rely on empirical models such as the Longo-Vaughan equation^{11,12} or an *a priori* assumption of a continuous distribution of work functions¹³ on the cathode surface. The construction of a fully physics-based model would enable the in-depth study and understanding of the physical factors determining the characteristics of the emission current density as a function of temperature and applied voltage. These factors include the impact of not only the number, range, and distribution of the work function values on a cathode surface but also the sizes, shapes, and spatial arrangement of different work function patches. In turn, understanding the impact of these physical effects would be instrumental in advancing the state of understanding of the interplay of emission physics, cathode materials engineering, and design of devices employing electron emission cathodes.

Experimental results including thermionic electron emission microscopy (THEEM) images reveal that polycrystalline cathodes have a spatial distribution of work function and emit non-uniformly.^{14–17} It is known that the non-uniform thermionic emission in a parallel diode is subject to the effects of 3-D space charge¹⁸, patch fields^{14,15}, Schottky barrier lowering⁵, and the lateral motion of electrons^{18,19}. Each of these effects has been studied in detail separately. While there is still no general, physics-based model unifying all of these effects, previous efforts have made advances in combining some subsets of the effects together. For example, the theory of the anomalous Schottky effect unifies the effects of patch fields and Schottky barrier lowering,²⁰ and a recent study by Chernin *et al.*¹⁸ discusses the effects of 3-D space charge and the lateral motion

of electrons. A key result from the work of Chernin *et al.* is that the lateral motion of electrons has a minor effect on predictions of averaged emission current density when 3-D space charge effect is considered. Therefore, it is sufficiently accurate to predict the averaged emission current density under the assumption that the electrons are restricted to move one-dimensionally from cathode to the anode with no lateral momentum, which is equivalent to assuming an infinite magnetic field. In this article, we unify the effects of 3-D space charge, patch field, Schottky barrier lowering, and, based on the work from Chernin *et al.*, neglect the lateral motion of electrons. We develop a model for the non-uniform thermionic emission from a heterogeneous surface in a perfect infinite parallel diode, and show that when correctly treated a relatively simple heterogeneous surface results in smooth and gradual TL-FSCL transitions as observed in experimental Miram curves and $I - V$ curves.

For the model of thermionic emission from heterogeneous surfaces developed in this work, the cathode is located at $z = 0$, and the anode at $z = d$, where d is the anode-cathode distance. It is assumed that the distribution of the electron energies follows a Maxwell-Boltzmann distribution, and that motion of the electrons between the cathode and the anode follows non-relativistic classical electrodynamic behavior. The total energy for each electron is conserved: $E = E_p(x, y, z) + mv^2/2$, where $E_p(x, y, z)$ is the potential energy at position (x, y, z) , m is the mass of an electron, v is the velocity. In the absence of an energy barrier at the surface of the cathode, the emission current density J due to the electrons with energy between E and $E + dE$ is:¹⁰

$$dJ(x, y; E) = \frac{AT}{k} \exp\left(-\frac{E - E_F(x, y)}{kT}\right) dE, \quad (1)$$

where $A = 4\pi me k^2/h^3$ is the Richardson constant, e is elementary charge, k is Boltzmann's constant, h is Planck's constant, T is temperature, and $E_F(x, y)$ is the local Fermi energy level of the cathode.

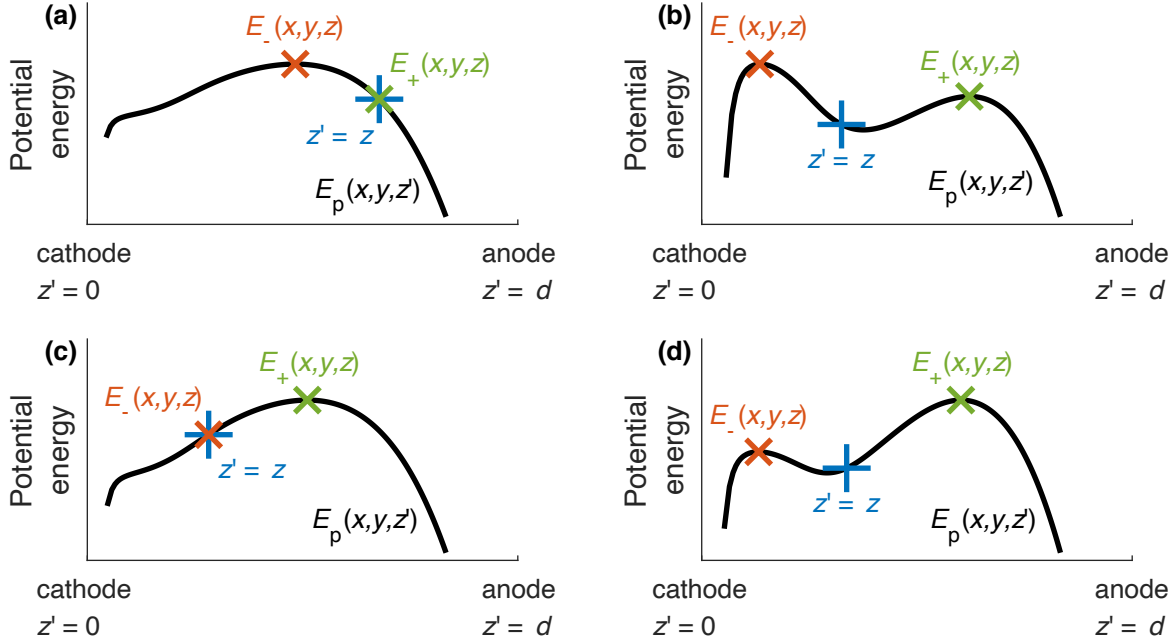


Figure 1. Sketch of the potential energy $E_p(x, y, z')$ for a given (x, y) as a function of z' (black curve). For a given position (x, y, z) (blue plus mark), its cathode-side barrier $E_-(x, y, z)$ is marked as red cross, and its anode-side barrier $E_+(x, y, z)$ as green cross. (a) and (b) are examples for the case of $E_-(x, y, z) \geq E_+(x, y, z)$, while (c) and (d) for $E_-(x, y, z) < E_+(x, y, z)$.

Figure 1 shows sketches of the potential energy $E_p(x, y, z')$ for a given (x, y) as a function of z' for different cases. For a given position (x, y, z) , we define its cathode-side barrier as $E_-(x, y, z) = \max_{0 \leq z' \leq z} E_p(x, y, z')$ and anode-side barrier as $E_+(x, y, z) = \max_{z \leq z' \leq d} E_p(x, y, z')$. The values of E_- and E_+ determine how many electrons are able to reach the position (x, y, z) , in the case that the lateral motion of electrons is neglected.

Considering the positions (x, y, z) satisfying $E_-(x, y, z) \geq E_+(x, y, z)$, electrons emitted from the cathode surface at position $(x, y, 0)$ with energy $E \geq E_-$ can pass through the cathode-side barrier and reach the position (x, y, z) as they move toward the anode. The charge density for positions (x, y, z) where $E_-(x, y, z) \geq E_+(x, y, z)$ has the form:

$$\rho(x, y, z) = - \int_{E=E_-}^{\infty} \frac{dJ}{v} = - \int_{E=E_-}^{\infty} \frac{dJ}{\sqrt{2(E-E_p)/m}}, \quad E_-(x, y, z) \geq E_+(x, y, z), \quad (2)$$

where the electron velocity $v = \sqrt{2(E - E_p)/m}$.

However, for any position (x, y, z) where $E_-(x, y, z) < E_+(x, y, z)$, electrons emitted from the cathode surface at $(x, y, 0)$ with energy $E \geq E_-$ can still pass through the cathode-side barrier and reach the position (x, y, z) . Electrons with energy $E_- \leq E < E_+$ will be reflected back

toward the cathode by the higher anode-side barrier and pass through the location (x, y, z) , this time moving back toward the cathode. Therefore, the charge density for positions (x, y, z) where $E_-(x, y, z) < E_+(x, y, z)$ has the form:

$$\rho(x, y, z) = - \left[\int_{E=E_-}^{\infty} \frac{dJ}{\sqrt{2(E-E_p)/m}} + \int_{E=E_-}^{E_+} \frac{dJ}{\sqrt{2(E-E_p)/m}} \right], \quad E_-(x, y, z) < E_+(x, y, z), \quad (3)$$

Substituting Equation 1 into Equations 2 and 3, we obtain a closed-form expression of the relation between the potential energy $E_p(x, y, z)$ and the charge density $\rho(x, y, z)$:

$$\rho(x, y, z) = \begin{cases} -\sqrt{\frac{\pi m}{2kT}} AT^2 \exp\left(-\frac{E_p(x, y, z) - E_F(x, y)}{kT}\right) \operatorname{erfc}\left(\sqrt{\frac{E_-(x, y, z) - E_p(x, y, z)}{kT}}\right), & E_-(x, y, z) \geq E_+(x, y, z) \\ -\sqrt{\frac{\pi m}{2kT}} AT^2 \exp\left(-\frac{E_p(x, y, z) - E_F(x, y)}{kT}\right) \left[2 \operatorname{erfc}\left(\sqrt{\frac{E_-(x, y, z) - E_p(x, y, z)}{kT}}\right) - \operatorname{erfc}\left(\sqrt{\frac{E_+(x, y, z) - E_p(x, y, z)}{kT}}\right) \right], & E_-(x, y, z) < E_+(x, y, z) \end{cases}, \quad (4)$$

where erfc is the complementary error function.

The electrostatic potential V and the charge density ρ satisfy Poisson's equation, and therefore the 3-D space charge effect is included in this model:

$$\nabla^2 V(x, y, z) = -\frac{\rho(x, y, z)}{\epsilon_0}, \quad (5)$$

where ϵ_0 is the vacuum permittivity.

The boundary condition for the cathode surface is^{10,20-22}

$$V(x, y, z = 0) = -\frac{E_F(x, y) + \phi(x, y)}{e}, \quad (6)$$

where $E_F(x, y)$ and $\phi(x, y)$ are the local Fermi level and the local work function of the cathode, respectively.

Similarly, the boundary condition for the anode surface is¹⁰

$$V(x, y, z = d) = -\frac{E_{F,\text{anode}}(x, y) + \phi_{\text{anode}}(x, y)}{e}, \quad (7)$$

where $E_{F,\text{anode}}(x, y)$ and $\phi_{\text{anode}}(x, y)$ are the local Fermi level and the local work function of the anode, respectively.

At thermodynamic equilibrium, the Fermi level is equal throughout a conductor. In the case of a conductive cathode and a conductive anode, $E_F(x, y)$ is a constant value throughout the cathode and $E_{F,\text{anode}}(x, y)$ is a constant value throughout the anode. Although the cathode is at a higher temperature than other parts in typical operating conditions, the extra voltage between the cathode and the anode due to the thermoelectric effect is in the scale of tens of millivolts, which is negligible compared with the applied voltage between the cathode and the anode V_{AK} , which is usually in the scales of hundreds of volts or higher. Neglecting the thermoelectric effect, the anode-

cathode Fermi level difference is $E_{F,\text{anode}} - E_F = -eV_{\text{AK}}$, where V_{AK} is the anode-cathode voltage as measured by a voltmeter in experiments. For the present model if we let $E_F = 0$ then $E_{F,\text{anode}} = -eV_{\text{AK}}$. In this case, the boundary conditions are $V(x, y, z = 0) = -\phi(x, y)/e$ and $V(x, y, z = d) = V_{\text{AK}} - \phi_{\text{anode}}(x, y)/e$. The cathode surface is a non-equipotential surface, and the patch field effect is included.

Considering the Schottky effect near the cathode surface, the potential energy E_p takes the form:

$$E_p(x, y, z) = -eV(x, y, z) - \frac{e^2}{16\pi\epsilon_0 z}, \quad (8)$$

where $-e^2/(16\pi\epsilon_0 z)$ is the energy term representing the image charge effect.

The non-uniform thermionic emission model can be solved by solving the system of Equations 4-8. A numerical method to solve this system of nonlinear equations is to solve them by iterations of $E_p \rightarrow \rho \rightarrow V \rightarrow E_p$ until convergence is obtained. One of the algorithms to solve the Poisson's equation in the step $\rho \rightarrow V$ involves a Fourier transformation for the x and y directions and the Thomas algorithm for the z direction.¹⁸ Once $E_p(x, y, z)$ is solved, one is able to calculate the maximum barrier $E_{p,\text{max}}(x, y) = \max_{0 \leq z \leq d} E_p(x, y, z)$, and the corresponding emission current density $J(x, y) = AT^2 \exp[-E_{p,\text{max}}(x, y)/(k_B T)]$. The averaged emission current density of the cathode can be obtained by averaging $J(x, y)$ over the whole cathode surface.

In the following results, we assess the predicted emission from our model and evaluate how each physical effect impacts the emission by comparing the results for the cases where some subset or all of the three physical effects are considered. The no-patch-field results are obtained under the assumption that the cathode surface is an equipotential surface, which, without loss of generality, is assumed to be zero, i.e. $V(x, y, z = 0) = 0$, and therefore $E_F(x, y) = -\phi(x, y)$, and the potential of the anode surface is assumed to be $V(x, y, z = d) = V_{\text{AK}}$. The results without the Schottky effect are obtained by omitting the image charge term $-e^2/(16\pi\epsilon_0 z)$ in Equation 8. The results without space charge are obtained by solving the maximum barrier $E_{p,\text{max}}(x, y)$ at zero temperature when there is no space charge, with the assumption that the maximum barrier $E_{p,\text{max}}(x, y)$ remains the same at finite temperatures. The results considering the 1-D space charge effect without the patch field effect are obtained under the assumption that each patch emits independently, where we replace the 3-D Laplace operator ∇^2 in Equation 5 with the

corresponding 1-D operator $\partial^2/\partial z^2$. The results considering the 1-D space charge effect with the patch field effect are obtained in the following order: (1) Solve the model with patch fields included at zero temperature to get the potential energy E_{p1} . (2) Solve the model without patch field effects at zero temperature to get the potential E_{p2} . (3) Assume the additional potential energy due to patch field is $E_{PF} = E_{p1} - E_{p2}$. (4) Solve the model after replacing the 3-D Laplace operator ∇^2 in Equation 5 with the corresponding 1-D operator $\partial^2/\partial z^2$ and adding a term E_{PF} to the right side of Equation 8.

In this work, we use a model heterogeneous surface characterized by a checkerboard spatial distribution of work functions, as shown in **Figure 2**. Similar checkerboard distributions have been used in many previous studies of non-uniform emission.^{14,15,23,24} Here, a checkerboard model surface with work function values of $\phi_1 = 2$ eV and $\phi_2 = 2.5$ eV and with square size $a = 5 \mu\text{m}$ is used. These work function values are typical values for sintered porous tungsten (dispenser) cathodes and the square size is the typical grain size.^{2,19,25,26} The anode-cathode distance d is chosen to be 1 mm. To better compare the model results with and without the inclusion of the patch field effect, it is assumed that the anode has a work function of 2.25 eV, equal to the mean work function of the cathode. Under this assumption, the averaged voltage between the cathode surface and the anode surface is V_{AK} for both cases.

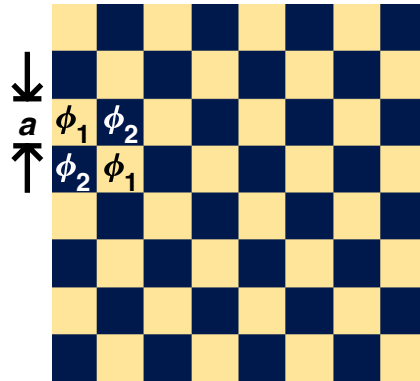


Figure 2. Model heterogeneous emission surface characterized as a checkerboard of spatial distributions of work function. In this work, values of $\phi_1 = 2$ eV and $\phi_2 = 2.5$ eV and square size $a = 5 \mu\text{m}$ are used.

Figure 3 contains predicted $J - T$ (Miram) and $J - V$ (or $I - V$) curves separately showing the effect of space charge at the level of 1-D and 3-D, patch fields, and Schottky barrier lowering on the resulting emission current density. From **Figure 3**, some qualitative, general features of the current density as a function of T and V emerge based on the inclusion of different

physical effects. The inclusion of space charge effects reduces the total emission, where 1-D space charge results in greater reduction in total emission than 3-D space charge. The inclusion of patch fields also reduces the total emission. Finally, the Schottky effect increases the emission by reducing the emission surface barrier. These general findings are consistent with a number of previous studies^{5,7-10,18}.

In the predicted $J - T$ curves (**Figure 3a**), all of the $J - T$ curves with no space charge effects (dotted curves) increase exponentially. This behavior occurs regardless if the patch field and Schottky effects are considered, and approximately follows the behavior of the Richardson-Dushman equation. Results of 1-D space charge without the patch field effect (dashed red and dashed blue curves) give peculiar stepped curves qualitatively inconsistent with experiment, calling into question the assumption that each patch emits independently. **Figures 3a** and **3c**, illustrate that the 3-D space charge effect itself (solid blue curve) does not make the TL-FSCL transition region smooth. However, smooth TL-FSCL transition regions are observed when both 3-D space charge and patch field effects are included together (solid green and solid yellow curves). Compared with space charge and patch field effects, the Schottky effect is minor in determining the shape of the $J - T$ curves, and only acts to make the transition slightly smoother (solid red vs. solid blue curves, and solid green vs. solid yellow curves, best observed in **Figure 3c**).

Figure 3b and **Figure 3d** show the predicted $J - V$ curves. In **Figure 3b** and **Figure 3d**, all curves without the Schottky effect (yellow and blue curves) converge to values one would obtain from the Richardson-Dushman equation at the TL regions (high voltage end). In addition, all curves with the Schottky effect included (green and red curves) show the asymptotic Schottky behavior of the current density at high voltages, as observed in experiments. The curves which ignore space charge effects (dotted curves) give the expected asymptotic behavior at the high voltage limit. Contrary to what was observed for the $J - T$ curves, the green, yellow, and red $J - V$ curves in **Figure 3b** and **Figure 3d** show that both patch field and Schottky effects contribute to the smoothness of the TL-FSCL transition. Although the behavior of the $J - T$ curves with 1-D space charge in **Figure 3a** differs substantially from typical experimental curves, the behavior of the $J - V$ curves with 1-D space charge effects in **Figure 3b** is qualitatively similar with the corresponding $J - V$ curves when 3-D space charge effects are included.

Both the $J - T$ and $J - V$ curves are commonly used to evaluate the cathode performance and it is therefore critical for an emission model to accurately predict the behavior of both curves.

Among the twelve cases plotted in **Figure 3**, only the case where all the effects of 3-D space charge, patch fields, and Schottky barrier lowering are considered (solid green curves) predicts a smooth $J - T$ (i.e., a smooth TL-FSCL transition with temperature and a smooth Miram curve knee) and $J - V$ curve with the Schottky behavior, thereby reproducing the known experimental cathode emission behavior as both a function of temperature and applied voltage.

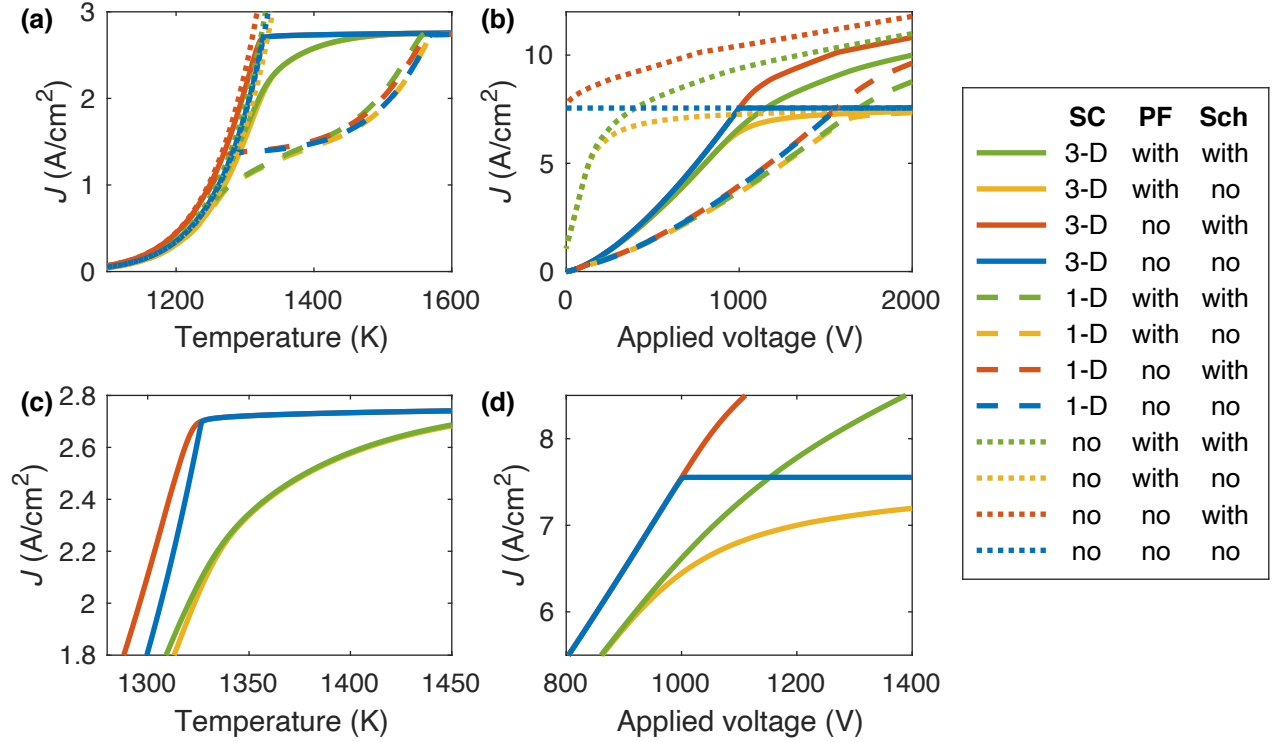


Figure 3. Predicted (a) $J - T$ (Miram) curves at applied voltage $V_{AK} = 500$ V and (b) $J - V$ curves at temperature $T = 1400$ K with various combinations of space charge (SC), patch field (PF), and Schottky barrier lowering (Sch) effects considered. (c) and (d) focus on the TL-FSCL transition region of (a) and (b), respectively, for the case of 3-D space charge with and without the effect of patch fields and Schottky barrier lowering. See the supplementary material for the data.

Overall, we have shown that for predicting $J - T$ curves, the space charge effect and the patch field effect each play a more important role than the Schottky effect in determining the shape of the TL-FSCL transition. On the other hand, for predicting $J - V$ curves, the Schottky effect is essential to predict asymptotic Schottky behavior of the current density at high voltages. Even with the simple heterogenous work function distribution considered in this work, consisting of only two discrete work function values, the predicted TL-FSCL transition regions are smooth for both the $J - T$ and $J - V$ curves, in agreement with experimental observations on real cathodes. The

present model results illustrate that neither empirical equations such as the Longo-Vaughan equation^{11,12} nor an *a priori* assumption of a continuous distribution of work functions on the emitting surface¹³ are necessary to generate a smooth TL-FSCL transition, assuming the effects of 3-D space charge, patch fields, and Schottky barrier lowering are all taken into consideration. This result demonstrates the value of the developed model in predicting the non-uniform thermionic emission from a heterogeneous cathode surface and suggests that the smooth behavior observed in experiments is consistent with relatively simple work function distributions on surfaces. Although the effects of space charge, patch fields, and Schottky barrier lowering have been studied separately, this work has unified all of these effects and applied the resulting model to predict the emission current density as a function of temperature and applied voltage for TL and FSCL regions, and, crucially, the transition region between TL and FSCL regions. We anticipate the emission model presented here will enable further explorations and understanding of the interplay of surface materials properties and physics of a cathode, not only including the distribution of the values of work function values but also their spatial arrangement, and the resulting engineering and design of an array of devices incorporating thermionic cathodes.

See the supplementary material for the data plotted in **Figure 3**.

This work was funded by the Defense Advanced Research Projects Agency (DARPA) through the Innovative Vacuum Electronic Science and Technology (INVEST) program.

References

- ¹ J.H. Booske, Phys. Plasmas **15**, 055502 (2008).
- ² J.-Y. Gao, Y.-F. Yang, X.-K. Zhang, S.-L. Li, P. Hu, and J.-S. Wang, Tungsten 1 (2020).
- ³ O.W. Richardson, J. Röntgen Soc. **18**, 150 (1922).
- ⁴ S. Dushman, Rev. Mod. Phys. **2**, 381 (1930).
- ⁵ W. Schottky, Zeitschrift Für Phys. **14**, 63 (1923).
- ⁶ C.D. Child, Phys. Rev. (Series I) **32**, 492 (1911).
- ⁷ I. Langmuir, Phys. Rev. **21**, 419 (1923).

- ⁸ T.C. Fry, *Phys. Rev.* **17**, 441 (1921).
- ⁹ J.B. Scott, *J. Appl. Phys.* **52**, 4406 (1981).
- ¹⁰ G. Eng, *J. Appl. Phys.* **58**, 4365 (1985).
- ¹¹ R.T. Longo, in *1980 Int. Electron Devices Meet.* (IRE, 1980), pp. 467–470.
- ¹² R. Vaughan, *IEEE Trans. Electron Devices* **33**, 1925 (1986).
- ¹³ C.E. Maloney and C.S. Fang, *Appl. Surf. Sci.* **24**, 407 (1985).
- ¹⁴ J.A. Becker, *Rev. Mod. Phys.* **7**, 95 (1935).
- ¹⁵ C. Herring and M.H. Nichols, *Rev. Mod. Phys.* **21**, 185 (1949).
- ¹⁶ G.A. Haas and R.E. Thomas, *J. Appl. Phys.* **38**, 3969 (1967).
- ¹⁷ D. Norman, R.A. Tuck, H.B. Skinner, P.J. Wadsworth, T.M. Gardiner, I.W. Owen, C.H. Richardson, and G. Thornton, *Phys. Rev. Lett.* **58**, 519 (1987).
- ¹⁸ D. Chernin, Y.Y. Lau, J.J. Petillo, S. Ovtchinnikov, D. Chen, A. Jassem, R. Jacobs, D. Morgan, and J.H. Booske, *IEEE Trans. Plasma Sci.* **48**, 146 (2020).
- ¹⁹ E.A. Adler and R.T. Longo, *J. Appl. Phys.* **59**, 1022 (1986).
- ²⁰ L.K. Hansen, *J. Appl. Phys.* **37**, 4498 (1966).
- ²¹ J. Trigueiro, N. Bundaleski, A.G. Silva, and O.M.N.D. Teodoro, *Vacuum* **98**, 41 (2013).
- ²² T. Schultz, T. Lenz, N. Kotadiya, G. Heimel, G. Glasser, R. Berger, P.W.M. Blom, P. Amsalem, D.M. de Leeuw, and N. Koch, *Adv. Mater. Interfaces* **4**, 1 (2017).
- ²³ K.T. Compton and I. Langmuir, *Rev. Mod. Phys.* **2**, 123 (1930).
- ²⁴ W.B. Nottingham, *Phys. Rev.* **49**, 78 (1936).
- ²⁵ R. Jacobs, D. Morgan, and J. Booske, *APL Mater.* **5**, 116105 (2017).
- ²⁶ D.M. Kirkwood, S.J. Gross, T.J. Balk, M.J. Beck, J. Booske, D. Busbaher, R. Jacobs, M.E. Kordesch, B. Mitsdarffer, D. Morgan, W.D. Palmer, B. Vancil, and J.E. Yater, *IEEE Trans.*

Electron Devices **65**, 2061 (2018).